Research Article Vol. 57, No. 10 / 1 April 2018 / Applied Optics 2647

applied optics

Design and analysis of a worm gear turntable off-axis assembly method in a three-grating monochromator

Jianjun Chen,[1,2] Jicheng Cui,[1,*] Xuefeng Yao,[1,2] Jianan Liu,[1,2] and Ci Sun[1]

[1]National Engineering Research Centre for Diffraction Gratings Manufacturing and Application, Changchun Institute of Optics, Fine Mechanics and Physics, Chinese Academy of Sciences, Changchun, Jilin 130033, China
[2]Daheng College, University of Chinese Academy of Sciences, Beijing 100049, China
*Corresponding author: jicheng_cui@163.com

Received 9 October 2017; revised 25 January 2018; accepted 30 January 2018; posted 30 January 2018 (Doc. ID 308375); published 29 March 2018

To solve the problem where the actual grating aperture decreases with an increasing scanning angle during the scanning of a three-grating monochromator, we propose an off-axis assembly method for the worm gear turntable that makes it possible to suppress this aperture reduction. We simulated and compared the traditional assembly method with the off-axis assembly method in the three-grating monochromator. Results show that the actual grating aperture can be improved by the off-axis assembly method. In fact, for any one of the three gratings, when the monochromator outputs the longest wavelength in the corresponding wavelength band, the actual grating aperture increases by 45.93%. Over the entire monochromator output band, the actual grating aperture increased by an average of 32.56% and can thus improve the monochromator's output energy. Improvement of the actual grating aperture can also reduce the stray light intensity in the monochromator and improve its output signal-to-noise ratio.

OCIS codes: (050.0050) Diffraction and gratings; (120.4640) Optical instruments; (300.6320) Spectroscopy, high-resolution.

https://doi.org/10.1364/AO.57.002647

1. INTRODUCTION

The monochromator is the basic optical instrument in the fields of spectral measurement and spectral analysis, and has a wide range of applications in physics, chemistry, biology, medicine, environmental protection, and industrial chemistry [1–4]. Monochromators can be divided into grating-type and prism-type instruments based on the different dispersion elements that they use. Grating monochromators are widely used because of their uniform dispersion, high spectral resolution, and several other advantages [5]. Wavelength scanning is realized by rotation of the grating in a grating monochromator, and different rotation angles correspond to different monochromatic light wavelengths [6]. Monochromators can be used to analyze the absorption spectra of transparent objects and solutions to determine their compositions [7–9], and can analyze emission spectra to determine the energy distributions in these spectra [10–12]. In addition, high spectral resolution monochromators can be used to perform wavelength calibration for other spectroscopic instruments [13–15].

The spectral resolution and the wavelength range of the grating monochromator, however, are contradictory [16]. To ensure high spectral resolution, a grating monochromator cannot output a wide band of monochromatic light, and it is difficult to use a single grating to achieve high diffraction efficiency over a wideband range; therefore, to output high-resolution and wideband monochromatic light simultaneously, multigrating switching is necessary [17–19].

In traditional monochromator systems, scanning of a single grating can be performed using a sine bar mechanism [20] in which the center of the grating acts as the center of rotation. However, in a monochromator system using multigrating switching, a worm gear scanning mechanism [21] is required because it can rotate through 360° and achieve its intended purpose of grating switching and scanning, so the scanning axis is out of the grating plane, and, as a result, it brings two changes to the optical system. One change is the distance between the grating and the collimator during the worm gear scanning process. However, since the collimation beam from the collimator is parallel light, and the value of this change is very small relative to the distance between the grating and the collimator, the influence of the position of the grating on the actual aberration can be ignored. Of course, the impact on the monochromator resolution is also extremely limited. Another change is that the full aperture of the grating cannot always be present in the

collimated beam during scanning of the worm gear turntable. This means that the actual grating aperture is smaller than the theoretical aperture in the optical design. As a result, all of the energy of the collimated beam cannot enter the subsequent optical system, meaning that the monochromator output energy will be reduced. Additionally, the light in the collimated beam that does not enter the subsequent path will be directed toward the inner walls of the instrument, thus increasing the stray light. Accordingly, during use, the output energy of the monochromator is reduced while the stray light is increased, which means that the signal-to-noise ratio of the instrument is reduced, leading to reduced accuracy in the spectral analysis.

With regard to the loss of the actual grating aperture during the grating scanning process in a three-grating switching scanning monochromator system, we propose the use of the worm gear turntable off-axis assembly method to suppress aperture reduction during the scanning process and thus ensure the actual monochromator performance. Using a three-grating scanning monochromator that was designed for the wavelength calibration of imaging spectrometers, we have performed accurate theoretical calculations and simulations, and the changes in the actual grating aperture during the grating scanning process are compared for worm gear turntables that use the traditional assembly method and the off-axis assembly method. The results show that the worm gear turntable off-axis assembly method can be highly effective in suppressing the reduction of both the actual grating aperture and the output energy, and can also reduce the stray light in the instrument, thus improving the system's output signal-to-noise ratio.

2. COMPARISON OF THE TWO WORM GEAR TURNTABLE ASSEMBLY METHODS IN A THREE-GRATING MONOCHROMATOR

A wideband and high-resolution three-grating monochromator was designed to perform wavelength calibration of an imaging spectrometer. The grating densities of the three gratings, designated G1, G2, and G3, used in this monochromator are 2400 gr/mm, 1200 gr/mm, and 600 gr/mm, respectively, and these densities correspond to monochromatic light outputs in the 280 nm–560 nm, 560 nm–1120 nm, and 1120 nm–2240 nm ranges, respectively. Typically, we only analyze the conditions of the grating G1 in this work.

A schematic diagram of this three-grating monochromator is shown in Fig. 1. In Fig. 1(a), the worm gear is traditionally assembled [i.e., the rotation center O of the worm gear turntable to which the gratings are fixed is located on the central axis of the system (Fig. 1(a), dashed line)]. When the worm gear turntable rotates, G1 can be scanned, or the other gratings can be switched into its position for operation. In Fig. 1(b), the worm gear is assembled off-axis, so the rotation center O′ of the worm gear turntable is not located on the central axis of the system and has been shifted relative to the central axis of the system.

When the grating rotation angle $\varphi = 0$, the grating is located at the initial position. When the monochromator operates from the initial position, the worm gear rotates clockwise, and as shown in Fig. 1(a), the actual aperture of grating G1 decreases monotonically with increasing grating angle;

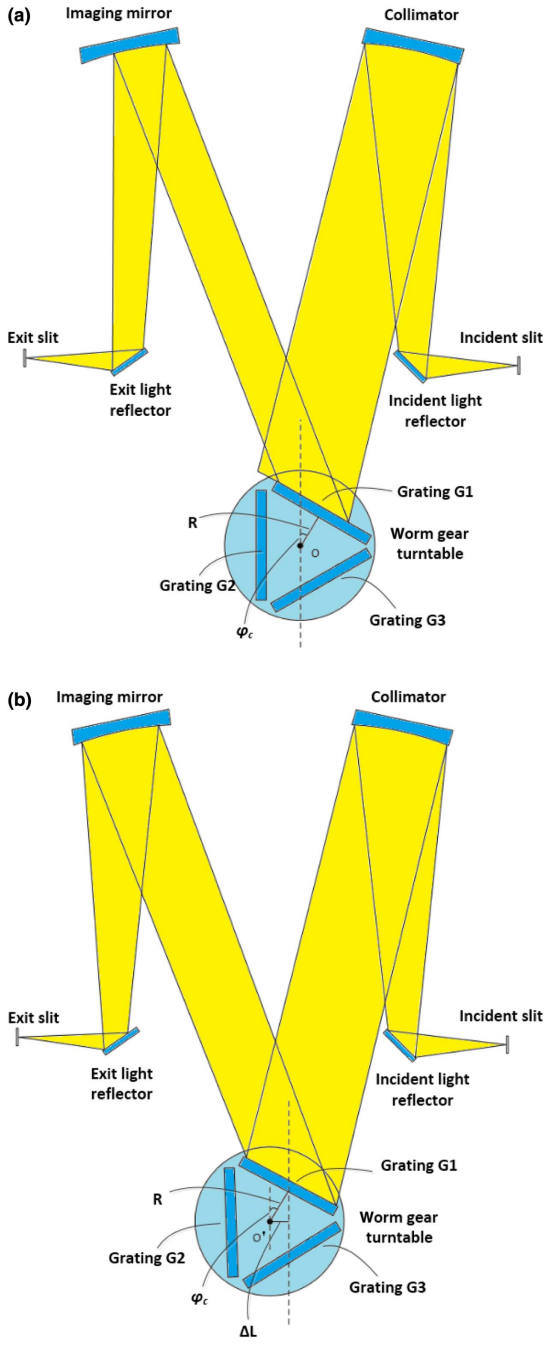

Fig. 1. Schematic diagram of the three-grating monochromator.

however, in Fig. 1(b), the actual aperture of G1 increases with increasing grating angle, and then decreases with an increase in the grating angle. This intuitive idea serves as the inspiration for the proposed worm gear turntable off-axis assembly method.

The core concept of the worm gear turntable off-axis assembly method is that when the grating rotates to an angle that corresponds to the center wavelength, the grating center is then located on the central axis of the system. In other words, when the monochromator output is at its center wavelength, the grating is in the theoretical position from the optical design. Therefore, the reduction in the actual grating aperture can be

suppressed across the entire working angle range, and the degree of actual aperture reduction at the edge wavelength can be balanced. Based on this idea, we can determine the turntable displacement by Fig. 1(b), the displacement is given by $\Delta L = R \times \sin \varphi_c$, where R is the radius from the center of the grating to the center of turntable (i.e., the radius of grating rotation), and φ_c is the grating angle that corresponds to the central wavelength (i.e., the displacement of the worm gear turntable relative to the center axis of the system is ΔL).

3. THEORETICAL CALCULATION OF THE ACTUAL GRATING APERTURE IN THE TRADITIONAL ASSEMBLY METHOD

Using the geometric abstraction concept, we can simplify the worm gear turntable part of Fig. 1 to give the form shown in Fig. 2, where grating G1 is abstracted as the line segment AB, and the two edge rays of the collimated beam are straight lines L_1 and L_2. The grating is filled with collimated beams in the initial position, but when the turntable rotates clockwise, a portion of the grating will obviously roll outside the collimated beam's range.

In Fig. 2, a Cartesian coordinate system is established to quantify the loss of the grating aperture. The rotating center O of the turntable is used as the origin of the coordinate system, where the horizontal and vertical directions are the x and y axes, respectively. It is easy to see that point B tracks a circular arc during the grating scanning with respect to the center of the circle as the coordinate system origin, with a radius of L_{OB}. Thus, we can obtain this parameter equation for the circle,

$$x = L_{OB} \times \cos\theta \qquad y = L_{OB} \times \sin\theta. \tag{1}$$

Here, θ is the circle equation parameter. Based on the geometric relationship shown in Fig. 2, we obtain

$$\theta + \varphi + \arctan\left(\frac{L}{2R}\right) = 90°. \tag{2}$$

When the grating angle is φ, the coordinates of point B can then be written as

$$x_B = L_{OB} \times \cos\left(90° - \varphi - \arctan\frac{L}{2R}\right)$$
$$y_B = L_{OB} \times \sin\left(90° - \varphi - \arctan\frac{L}{2R}\right). \tag{3}$$

At this point, the slope of the line l, at which the grating is located, is given by $\tan(180° - \varphi)$, and thus the linear equation is

$$y = \tan(180° - \varphi) \times x + L_{OB} \times \sin\left(90° - \varphi - \arctan\frac{L}{2R}\right) - \tan(180° - \varphi) \times L_{OB} \times \cos\left(90° - \varphi - \arctan\frac{L}{2R}\right). \tag{4}$$

If we assume that the eccentricity of the collimator is $\alpha/2$, then the slope of the collimated ray l_2 is $\tan(90° - \alpha)$. If the grating aperture is L, and the line segment AB, which represents the rotation radius of the grating, is R, then we can obtain the coordinates of point B as $(L/2, R)$. When the grating is at the initial position, then the linear L_2 equation is

$$y = \tan(90° - \alpha) \times x - \frac{L}{2} \times \tan(90° - \alpha) + R. \tag{5}$$

By combining Eqs. (4) and (5), the coordinates of the intersection point $M(x_M, y_M)$ of the line L and the collimated beam L_2 can be obtained; thus the reduced grating length L_{MB} (R, L, L_{OB}, α, and φ) during the scanning process is given by

$$L_{MB} = \sqrt{(x_M - x_B)^2 + (y_M - y_B)^2}. \tag{6}$$

In the three-grating monochromator, when the output wavelength range of grating G1 is 280 nm–560 nm, the corresponding grating angle φ is 19.95°–43.03°. The grating aperture L is 60 mm, and the grating rotation radius R is 30 mm, which means that $L_{OB} = 42.43$ mm. The eccentricity of the collimator is 4.5°; therefore, according to Eq. (6), we can obtain the actual grating aperture L_0' that corresponds to any grating angle φ, because $L_0' = L - L_{MB}$. The relationship between the grating rotation angle and the actual grating aperture is shown in Fig. 3. As we can see from the range of the monochromator working angle, the actual reduction in the grating aperture is

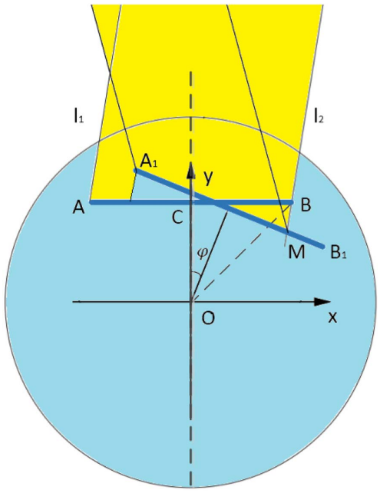

Fig. 2. Geometric abstraction schematic of the worm gear turntable components.

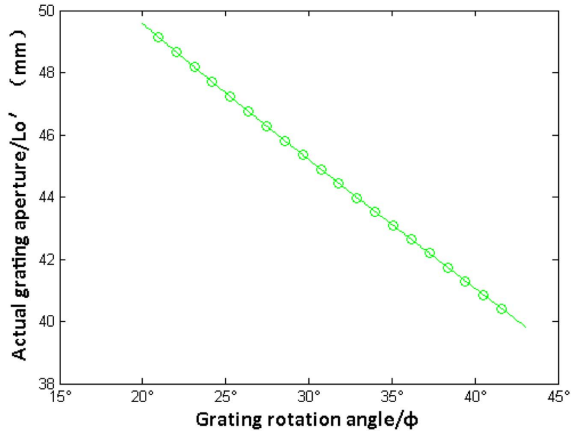

Fig. 3. Relationship curve between grating rotation angle and actual grating aperture.

close to linear. When the grating rotation angle $\varphi = 43.03°$ (i.e., at a monochromator output wavelength of 560 nm), the actual grating aperture is reduced to a minimum (i.e., $L_0' = 39.83$ mm). The resulting loss of the grating aperture is as high as 33.6%, and thus the actual monochromator performance will be seriously affected.

4. THEORETICAL CALCULATION OF THE ACTUAL GRATING APERTURE IN THE OFF-AXIS ASSEMBLY METHOD

We simulated the scanning process of the worm gear turntable off-axis assembly, and found that within its working angle range, the process of change in the actual grating aperture is roughly divided into three stages. These three stages are discussed in detail here.

A. First Stage

The geometric abstraction diagram of the first stage is shown in Fig. 4. The grating rotation angle range of the first stage is from 19.95° to the left edge of the grating, which is just covered by the collimated beam. Similarly, a planar coordinate system is used to solve for the grating angle of the critical state.

The rotating center of the off-axis worm gear turntable is O' $(-\Delta L, 0)$, and similarly, the track of point A is also a circular arc during the grating scanning. Therefore, the equation for the circle is

$$x = -\Delta L + L_{O'A} \times \cos\theta y = L_{O'A} \times \sin\theta, \tag{7}$$

where θ is the circle equation parameter. Based on the geometric relationship shown in Fig. 4, we obtain

$$\theta + \varphi + 90° - \arctan\left(\frac{L}{2R}\right) = 180°. \tag{8}$$

When the grating rotation angle is φ, the coordinates of point A can be obtained using Eq. (7),

$$x_A = -\Delta L + L_{O'A} \times \cos\theta_A \qquad y_A = L_{O'A} \times \sin\theta_A. \tag{9}$$

Of course, the slope of the collimated ray L_1 is $\tan(90° - \alpha)$, and the intersection between the line of the grating and the collimated light L_1 is at point D $(-L/2, R)$; therefore, the equation of the linear ray L_1 is

$$y = \tan(90° - \alpha) \times x + \frac{L}{2} \times \tan(90° - \alpha) + \mathrm{R}. \tag{10}$$

By substituting Eq. (9) into Eq. (10), we can obtain the intersection point between the collimated ray $L1$ and the scanning trajectory of point A, and the corresponding parameters are $\theta_A = 107.85°$ and $\theta_A = -125.85°$. Based on the geometric relationship shown in Fig. 5, $\theta_A = 107.85°$ is the desired angle, and we then can obtain the critical rotation angle for the first stage using Eq. (7). This critical rotation angle is $\varphi = 27.15°$, which means that the grating rotation angle range of the first stage is 19.95°–27.15°.

When the grating is at its initial position, the equation of the line l, where the grating is located, is $y = R$. The grating rotates around the point O' during the turntable scanning process, and when the grating rotation angle is φ, the slope of this line changes to $\tan 180° - \varphi$. At this point, the coordinates of point A on line l are

$$x_A = -\Delta L + L_{O'A} \times \cos\left(90° - \varphi + \arctan\frac{L}{2R}\right)$$
$$y_A = L_{O'A} \times \sin\left(90° - \varphi + \arctan\frac{L}{2R}\right). \tag{11}$$

Therefore, during the scanning process, the equation for line l can be expressed as

$$y = \tan(180° - \varphi) \times x + L_{O'A} \times \sin\left(90° - \varphi + \arctan\frac{L}{2R}\right)$$
$$- \tan(180° - \varphi) \times \left[-\Delta L + L_{O'A} \times \cos\left(90° - \varphi + \arctan\frac{L}{2R}\right)\right]. \tag{12}$$

By combining Eqs. (10) and (12), we can obtain the position coordinates of intersection point D, (x_D, y_D) during the scanning process. Then, by applying the two-point distance formula, we can obtain L_{AD} (i.e., in the first stage of the process of monochromator operation), and the reduction of the actual grating aperture is given by

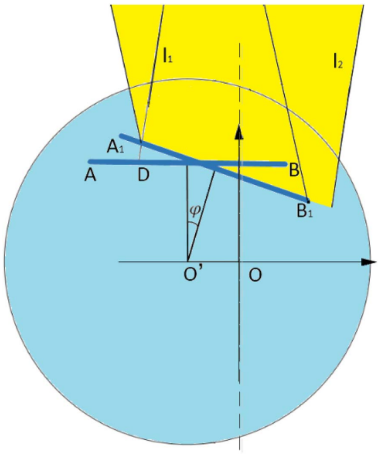

Fig. 4. Schematic diagram of the first stage of the scanning process.

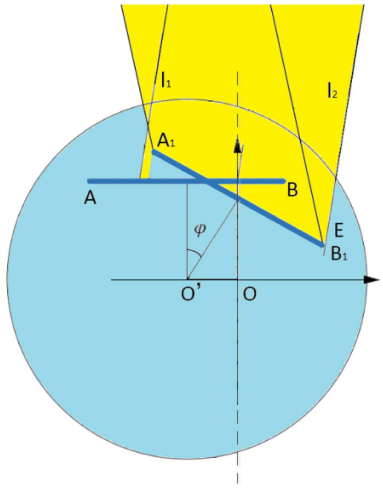

Fig. 5. Schematic diagram of the second stage of the scanning process.

$$L_{AD} = \sqrt{(x_D - x_A)^2 + (y_D - y_A)^2}. \quad (13)$$

B. Second Stage

The geometric abstraction diagram for the second stage is shown in Fig. 5. As the figure shows, at this stage, the left side of the grating has turned into the collimated beam range, while the right side has not yet turned out of range. This means that the entire grating is within the collimated beam range, and the critical state is thus at the right side of the grating, just at the right edge of the collimated beam.

The intersection E between the right end of the grating and the collimated ray L_2 is on the circle O'. The coordinates of E can then be written as

$$x_E = -\Delta L + L_{O'A} \times \cos\theta_E \qquad y_E = L_{O'A} \times \sin\theta_E. \quad (14)$$

By substituting Eq. (14) into Eq. (5), we can obtain $\theta_E = 10.06°$. Similarly, based on the geometric relationship shown in Fig. 5, we can determine that the critical rotation angle of the second stage is 34.94°, and thus the grating rotation angle range of the second stage is 27.15°–34.94°. In the second stage, the entire grating is located within the collimated beam range to participate in the dispersion process.

C. Third Stage

The grating rotation angle range of the third stage is 27.15°–34.94°, and the geometric abstraction diagram of the third stage is shown in Fig. 6.

In the third stage, the right edge of the grating turns such that it is located outside the collimated beam range, and the actual grating aperture decreases with an increasing grating rotation angle. If the equation of the line l, at which the grating is located during the scanning process, is combined with the equation of the collimated ray L2 [i.e., combined Eqs. (10) and (4)], we can obtain the coordinates of intersection $E(x_E, y_E)$. Therefore, during the third stage of the monochromator operation process, the reduction of the actual grating aperture is given by

$$L_{BE} = \sqrt{(x_E - x_B)^2 + (y_E - y_B)^2}. \quad (15)$$

We can summarize these three stages of the monochromator operation process, and the functional relationship between the

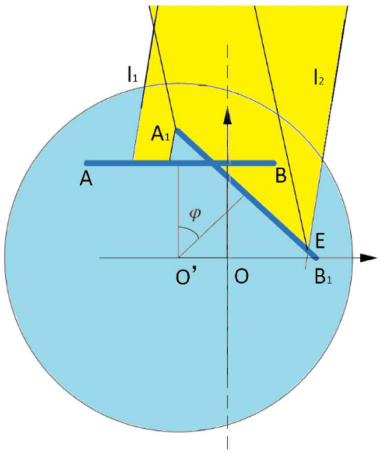

Fig. 6. Schematic diagram of the third stage of scanning process.

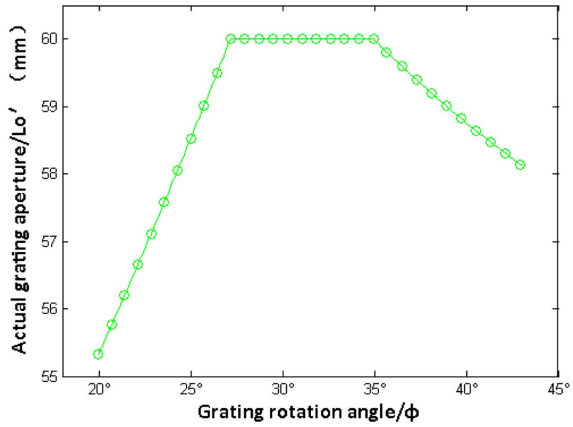

Fig. 7. Relationship curve between grating rotation angle and actual grating aperture.

actual grating aperture L' and the grating rotation angle is written in piecewise form as

$$L' = \begin{cases} L - L_{AD} & (19.95° < \varphi < 27.15°) \\ L & (27.15° < \varphi < 34.94°) \\ L - L_{BE} & (34.94° < \varphi < 43.03°) \end{cases}. \quad (16)$$

Therefore, during the monochromator operation process, we can obtain the actual grating aperture that corresponds to any given grating angle using Eq. (16). Figure 7 shows the functional relationship curve of Eq. (16). The figure shows that the worm gear turntable off-axis assembly method can ensure that the actual grating aperture loss is smaller than the loss when using the conventional method and the trend of the actual grating aperture with grating rotation angle is consistent with our simulation results. The maximum loss of the actual grating aperture is only 7.8%, and no aperture loss occurs when the output wavelength is close to the intermediate wavelength. Additionally, when the monochromator outputs both sides of the wavelength, the resulting aperture loss is more balanced.

5. CONTRAST AND ANALYSIS OF THE TWO ASSEMBLY METHODS

During the monochromator operation process, the proportion of the increase in the actual grating aperture when using the worm gear turntable off-axis assembly method compared to that when using the conventional assembly method is represented by K, and can be expressed as

$$k = \frac{L' - L'_0}{L'_0} \times 100\%. \quad (17)$$

Here, L'_0 is the actual grating aperture of the traditional assembly, L' is the actual grating aperture of the off-axis assembly, and the change curve of K with grating rotation angle φ is shown in Fig. 8. The figure shows that the worm gear turntable off-axis assembly method can increase the actual grating aperture across the entire monochromator working angle range. With increasing grating rotation angle, the increase in the aperture size becomes more obvious; when the monochromator outputs the longest wavelength in this wavelength band, the

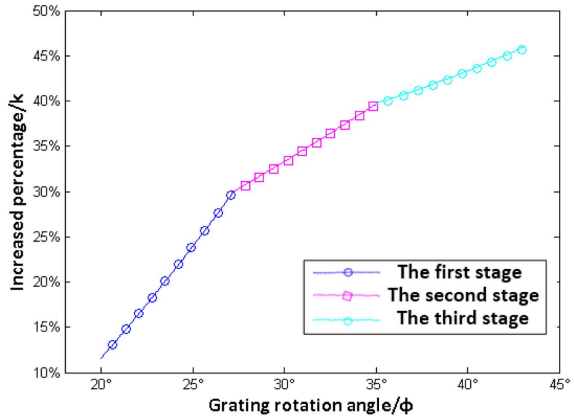

Fig. 8. Contrast curve of actual grating aperture between the conventional assembly method and the off-axis assembly method for the worm gear turntable.

actual grating aperture is increased by 45.93%. Over the entire output band, the actual grating aperture is increased by an average of 32.56%. While the above analysis was directed at grating G1, it is obvious that when the other gratings rotate to these positions, the same analysis is also applicable.

The improvement in the actual grating aperture means that more energy can enter the subsequent optical system, and thus the output energy of the monochromator improves remarkably. Simultaneously, the light within the collimated beam that cannot reach the grating will be reduced; this event will then reduce the stray light intensity within the instrument, and the output signal-to-noise ratio of the monochromator will also be improved.

6. CONCLUSION

In a three-grating monochromator using a worm gear as scanning mechanism, the traditional worm gear assembly method causes the monochromator to present actual grating aperture loss, and this loss is accompanied by an increase in the stray light intensity within the instrument. To address this problem, we proposed the worm gear off-axis assembly method. This method effectively suppresses the losses of the actual aperture during the scanning process, reduces the stray light intensity within the instrument, and thus improves the output signal-to-noise ratio. The worm gear turntable off-axis assembly method can not only be applied to the three-grating monochromator, but also can be used for other multigrating monochromators and similar spectrometers. Additionally, the required theoretical calculations and analyses for such applications can be performed using the method developed in this paper. This method can also serve as an inspiration for research and development of related spectral instruments.

Funding. National Major Scientific Instrument and Equipment Development Projects (2014YQ120351); Chinese Finance Ministry for the National R&D Projects for Key Science Foundation of China (NSFC) (61505204); Ministry of National Science and Technology for National Key Basic Research Program of China (2014CB049500); Changchun Science and Technology Project (12ZX23); Jilin Major Province Science & Technology Development Program Project (20140203011GX); Jilin Province Science & Technology Development Program Project in China (20170520167JH).

REFERENCES

1. B. H. Hamadani, J. Roller, and B. Dougherty, "Absolute spectral responsivity measurements of solar cells by a hybrid optical technique," Appl. Opt. **52**, 5184–5193 (2013).
2. S. Pedersen-Bjergaard and T. Greibrokk, "Evaluation of a low-resolution near-IR monochromator for atomic emission detection in capillary gas chromatography," J. Sep. Sci. **18**, 9–14 (2015).
3. L. A. Mackenzie and W. Frainbell, "The construction and development of a grating monochromator and its application to the study of the reaction of the skin to light," Br. J. Dermatol. **89**, 251–264 (1973).
4. H. Y. Liu, C. P. Ying, and K. F. Chen, *Research on Calibration Technology of the Wide Spectrum Grating Monochromator Wavelength Accuracy* (IEEE, 2016), pp. 1744–1747.
5. J. Zeng, Bayanheshig, and W. H. Li, "One step method to design concave holographic grating for monochromator," Spectrosc. Spect. Anal. **31**, 2586–2589 (2011).
6. O. Köysal, D. Önal, and S. Özder, "Thickness measurement of dielectric films by wavelength scanning method," Opt. Commun. **205**, 1–6 (2002).
7. J. Vattulainen, L. Wallenius, and J. Stenberg, "Experimental determination of SO2, C2H2, and O2 UV absorption cross sections at elevated temperatures and pressures," Appl. Spectrosc. **51**, 1311–1315 (1997).
8. H. J. Song, H. J. Shin, and M. K. Lee, "Photon energy calibration and measure of spectral resolving power of the monochromator by the use of N 1s NEXAFS from a solid sample," AIP. Conf. Proc. **705**, 561–563 (2004).
9. H. Edner, P. Ragnarson, and S. Spännare, "Differential optical absorption spectroscopy (DOAS) system for urban atmospheric pollution monitoring," Appl. Opt. **32**, 327 (1993).
10. G. W. Lee and S. K. Lee, "Observation of vibronic emission spectrum of jet-cooled duryl radical in corona excitation," J. Chem. Phys. **126**, 214308 (2007).
11. A. April and N. McCarthy, "Control of spectral aberrations in a monochromator using a plane holographic chirped grating," Appl. Opt. **47**, 2750 (2008).
12. J. A. Gardecki and M. Maroncelli, "Set of secondary emission standards for calibration of the spectral responsivity in emission spectroscopy," Appl. Spectrosc. **52**, 1179–1189 (1998).
13. R. A. Barnes, S. W. Brown, and K. R. Lykke, "Comparison of two methodologies for calibrating satellite instruments in the visible and near infrared," Appl. Opt. **54**, 10376–10396 (2015).
14. H. X. Cao, N. Wu, S. L. Feng, M. Z. Pan, Y. C. Zhang, and J. C. Cui, "Cross-spectral calibration for monochromator and imaging spectrometer," Opt. Precis. Eng. **22**, 2585–2591 (2014).
15. M. Lindrum and B. Nickel, "Wavelength calibration of optical multichannel detectors in combination with single- and double-grating monochromators," Appl. Spectrosc. **43**, 1427–1431 (1989).
16. A. Eberhagen, "A very rapidly scanning monochromator with low internal losses but high spectral resolution and repetition rate for millimetre and submillimetre wavelengths and below," Infrared Phys. **19**, 389–394 (1979).
17. Y. Gu, D. Qiao, and X. Xu, "Development of auto scanning multigrating monochromator," Chin. J. Sci. Instrum. **30**, 668–672 (2009).
18. T. Han, "New pattern monochromator of multi-grating using two-dimensional color CCD array," J. Infrared Millim. Waves **21**, 118–122 (2002).
19. S. H. Deng, "Development of intelligentized multi-grating monochromator," J. Infrared Millim. Waves **21**, 133–137 (2002).
20. J. U. White, N. L. Alpert, and A. G. Debell, "Infrared grating spectrophotometer," J. Opt. Soc. Am. **47**, 358–360 (1957).
21. K. P. Yates and R. F. Buhl, "Recording vacuum infrared prism-grating spectrometer," J. Opt. Soc. Am. **45**, 192–199 (1955).